ADVANCED ENERGY & SUSTAINABILITY RESEARCH
Open Access
www.advenergysustres.com

Low-Temperature Protonic Ceramic Fuel Cells through Interfacial Engineering of Nanocrystalline $BaCe_{0.7}Zr_{0.1}Y_{0.1}Yb_{0.1}O_{3-\delta}$ Electrolytes

*Jun Gao, Yuqing Meng, Jack H. Duffy, and Kyle S. Brinkman**

Nanocrystalline $BaCe_{0.7}Zr_{0.1}Y_{0.1}Yb_{0.1}O_{3-\delta}$ (BCZYYb) is designed by a novel strategy with improved proton transport properties at low temperatures ($<300\,°C$). In situ Raman spectroscopy and electrical conductivity relaxation (ECR) are used to quantitatively evaluate the surface exchange coefficients during the hydrogen isotope exchange process. Similar surface exchange coefficients are measured via in situ Raman spectroscopy and ECR measurements, representing new tools to better understand proton transport behaviors at the materials' interface. The surface exchange coefficient in nanocrystalline BCZYYb is nearly four times higher than that in conventional dense BCZYYb at 300 °C, indicating higher surface mobility of protonic species in the designed BCZYYb membrane. The improved performance originates from the combined interfacial and bulk effects for proton transport at low temperatures. In addition, low-temperature protonic ceramic fuel cells (PCFCs) are built based on a nanocrystalline BCZYYb electrolyte with improved single-cell performance at 300 °C, which indicates enhanced proton transport properties in contemporary energy conversion and storage materials can be achieved through interfacial engineering.

1. Introduction

Solid oxide fuel cells (SOFCs) are promising sustainable energy systems with high efficiency, fuel flexibility, and limited byproducts.[1–4] Despite their fundamental advantages, the reduction of SOFCs' operation temperature remains critical for their continued applications. Recently, protonic ceramic fuel cells (PCFCs) have received increased attention due to the lower migration energy of protons compared to oxygen ions.[5,6] The state-of-the-art protonic ceramic conductors in PCFCs are $BaZrO_3$ and $BaCeO_3$-based perovskite materials,[7–9] in which protons can be incorporated into the bulk materials as protonic defects ($OH_O^{\bullet}$) in the presence of water-vapor-containing gases. The formation of protonic defects occurs through Equation (1)

$$H_2O + V_O^{\bullet\bullet} + O_O^X \rightarrow 2OH_O^{\bullet} \tag{1}$$

For example, enhanced proton conductivity and sulfur tolerance were achieved for $BaCe_{0.7}Zr_{0.1}Y_{0.1}Yb_{0.1}O_{3-\delta}$ (BCZYYb).[8,11] Based on the $BaCe_{0.7}Zr_{0.1}Y_{0.1}Yb_{0.1}O_{3-\delta}$ electrolyte, Duan et al. developed high-performance protonic ceramic fuel cells and reversible protonic electrochemical cells.[5,6,12] Choi et al. reported a new stoichiometry, $BaCe_{0.4}Zr_{0.4}Y_{0.1}Yb_{0.1}O_{3-\delta}$, that exhibits enhanced CO_2 tolerance, likely due to its higher Zr content.[13] Demin and co-workers developed highly conductive and stable cerate–zirconate electrolytes of $BaCe_{0.5}Zr_{0.3}Ln_{0.2}O_{3-\delta}$ (where Ln = Dy, Sm, and Nd).[14–16] These materials exhibit very high bulk proton conductivity over a wide temperature range ($300\,°C < T < 700\,°C$).[10] However, their total conductivity is limited by the blocking effect of grain boundaries.[17] This effect originates from a positive excess charge at the grain boundary core, which leads to a depletion of mobile positive charge carriers ($OH_O^{\bullet}$, $V_O^{\bullet\bullet}$, $h^{\bullet}$) and an accumulation of negative carriers (such as e').

Great efforts have been devoted to manipulating the materials' interface with the aim of minimizing the grain boundary contribution. High proton conductivity was achieved in large-grained yttrium-doped barium zirconate, and the detrimental role of grain boundaries in these materials was confirmed by comparison of polycrystalline samples with different grain sizes.[18] Low-temperature proton conductivity was improved by up to 46 times in a BCZYYb membrane with nanoscale nickel metal thin film partially decorated grain boundaries.[19] Grain boundary resistance can be further minimized by fabricating highly textured yttrium-doped barium zirconate thin films with a grain-boundary-free structure through epitaxial growth or pulsed laser deposition.[20,21] Gang et al. revealed that ionic interface conduction, or surface diffusion, is the main ionic conduction mechanism in nanocrystalline $Ce_{0.8}Gd_{0.2}O_2$[22] and $BaZr_{0.9}Y_{0.1}O_{3-\delta}$[23] at high temperatures.

Parallel to bulk proton conduction improvement strategies, a new type of interfacial proton conduction was identified, relying

---

J. Gao, Dr. Y. Meng, J. H. Duffy, Prof. K. S. Brinkman
Department of Materials Science and Engineering
Clemson University
Clemson, SC 29634, USA
E-mail: ksbrink@clemson.edu

The ORCID identification number(s) for the author(s) of this article can be found under https://doi.org/10.1002/aesr.202100098.

DOI: 10.1002/aesr.202100098

on water absorption on the nanoscale membranes' interface (e.g., the surface and grain boundaries) at low temperatures.[24–26] Kim et al. developed water concentration cells using nanoscale fluorite-structured oxides as electrolytes for power generation at low temperatures.[27] The phenomenon has also been observed in other simple oxide systems, such as yttria-stabilized zirconia (YSZ),[28,29] titanium oxide,[30] and cerium oxide.[31,32]

Compared to simple oxides, however, less is known regarding proton transport through the interfaces in nanoscale perovskite membranes at low temperatures. In a recently published review,[33] proton transport behaviors in nanostructured simple oxides and perovskite materials were compared. At low temperatures ($<300\,°C$), proton transport relies on the novel use of interfacial hydrated layers in simple oxides. However, in nanostructured perovskite materials, protons transport not only through the hydrated layers in the interface, but also through the bulk material, indicating a new opportunity to develop a new type of protonic ceramic conductor with a combined "interfacial effect" and "bulk effect" for proton transport.

Isotope exchange methods are powerful tools to reveal information about surface reactions and transport in oxide materials.[34] For example, hydrogen diffusivities in the $La_{1-x}Sr_xScO_{3-\delta}$ oxides were determined by hydrogen isotope exchange and thermogravimetric analysis.[35] H_2/D_2 pulse isotope exchange experiments were used to obtain the surface exchange rate on a wide range of proton-conducting ceramics, suggesting similar surface composition leads to similar catalytic activity.[36] Prior work has quantitatively and kinetically described the isotope exchange process via in situ Raman spectroscopy to reveal the proton mobility on a nanostructured TiO_2 membrane's interface.[26]

In this work, we demonstrated a new strategy to enhance the proton transport properties in perovskite-based protonic ceramic conductors by the novel use of materials' interface. In situ Raman spectroscopy and electrical conductivity relaxation (ECR) were used to quantify the surface exchange coefficients during the hydrogen isotope exchange reactions. Higher surface exchange coefficients were achieved in our designed nanocrystalline membrane and excellent single-cell performance was demonstrated at 300 °C, indicating the interface can be used as an alternative pathway for proton transport at low temperatures in contrast to the conventional wisdom of interfacial blocking effect observed in high-temperature ionic conductors.

2. Results and Discussion

The X-ray diffraction pattern of the synthesized BCZYYb powder is shown on **Figure 1**a, Pure-phase BCZYYb was acquired above a calcination temperature of 1000 °C. Figure 1b displays the morphology of nanocrystalline BCZYYb by a dry-pressing method. No open pores are present in the membrane, and the grain size is less than 100 nm.

The surface exchange coefficients were first studied by in situ Raman spectroscopy to understand the proton transport in the designed nanocrystalline membrane. Raman spectra were obtained after switching the atmosphere from Ar–3% H_2O to Ar–3% D_2O at 300 °C. The hydrated interface contains chemisorbed and physiosorbed water layers, including free H_2O, hydrogen-bonded H_2O molecules, and surface-terminating hydroxyls.[24] The O—H vibration was immediately attenuated after introducing D_2O to the atmosphere, as shown in **Figure 2**a. The intensity of the ν_{OH} broad band at $\approx 3500\,cm^{-1}$ starts to decrease, and the intensity of the ν_{OD} broad band at $\approx 2500\,cm^{-1}$ starts to increase, both due to the isotope exchange reactions of proton-containing species on the membrane's interface. This phenomenon is consistent with previous reports of the hydrogen isotope exchange process.[24,26]

In the same manner, surface exchange coefficients during the hydrogen isotope exchange process were measured from 300 to 100 °C with a step of 50 °C. During the H/D exchange process, the relevant variable was the remaining OH existing on the surface and grain boundary interfaces, which was experimentally determined in terms of $I_{OH}/I_{OH_{initial}}$. As shown in Figure 2c, the decrease in ν_{OH} integrated intensity follows a straight line in the semilogarithmic plot. It is possible to define the first-order rate constant and surface exchange coefficient $k_{H/D}$, as described in previously published literature.[26,37,38]

Temperature-dependent measurements indicate that exchange rates were appreciably faster at elevated temperatures. For example, the surface exchange coefficients were $1.07 \times 10^{-4}\,s^{-1}$ and $1.37 \times 10^{-4}\,s^{-1}$ at 100 and 150 °C, respectively, which are very close to the measured surface exchange coefficients through ECR measurements by calculating the derivation of the electrical relaxation conductivity curve, as shown in Figure S1, Supporting Information. The conductivity and protons (in the form of OH) can be expressed as Equation (2), in which e is the electron charge, C is the proton concentration, and μ_{OH} is the mobility. Ideally, the mobility and diffusivity are independent of the concentration; thus, it will help to treat the concentration and transport separately.[39] The mobility can be calculated by the derivation of the electrical relaxation conductivity curve.

$$\sigma_{OH} = eC_{OH}\mu_{OH} = \frac{e^2 C_{OH}}{kT} D^0_{OH} \exp\left(\frac{-\Delta H_{m,OH}}{kT}\right) \tag{2}$$

To compare with the nanocrystalline BCZYYb membrane, a conventional BCZYYb membrane was fabricated by a two-step sintering method to achieve a fully dense membrane with grain size ≈500 nm, as shown in Figure S2, Supporting Information.

The Raman spectra of the dense BCZYYb membrane is shows in Figure S3, Supporting Information. The doublets around $350\,cm^{-1}$ (ν_1, ν_2) and the broad peak around $650\,cm^{-1}$ (ν_4) are associated with the stretching modes between B-site cations (Ce, Zr, Y, or Yb), and the peak around $430\,cm^{-1}$ (ν_3) is related to the symmetrical radial breathing of the oxygen surrounding the B-site cation.[40,41]

Surface exchange coefficients were also measured for the dense BCZYYb membrane using in situ Raman spectroscopy in the temperature range of 400–600 °C to match the working temperature of well-studied PCFCs. The representative temporal evolution of Raman spectra was acquired after changing the atmosphere from Ar–3% H_2O to Ar–3% D_2O at 400 °C, as shown in Figure 2b. The resulting integrated intensity as a function of time is shown in Figure 2d at different temperatures. Similar trends exist in the dense membrane as observed in the previously described nanocrystalline BCZYYb membranes.

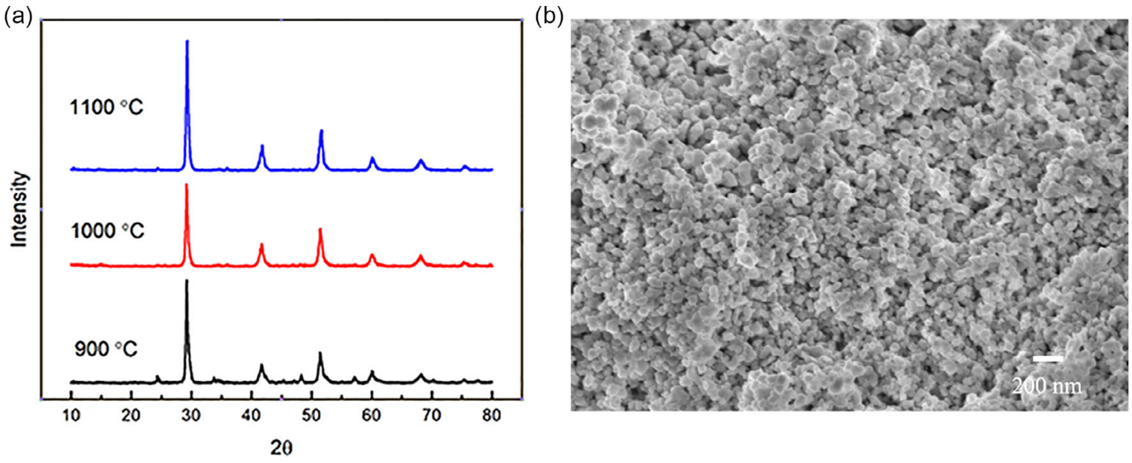

Figure 1. a) XRD patterns of BCZYYb powder calcined at different temperatures. b) Morphology of nanocrystalline BCZYYb membrane by a dry-pressing method.

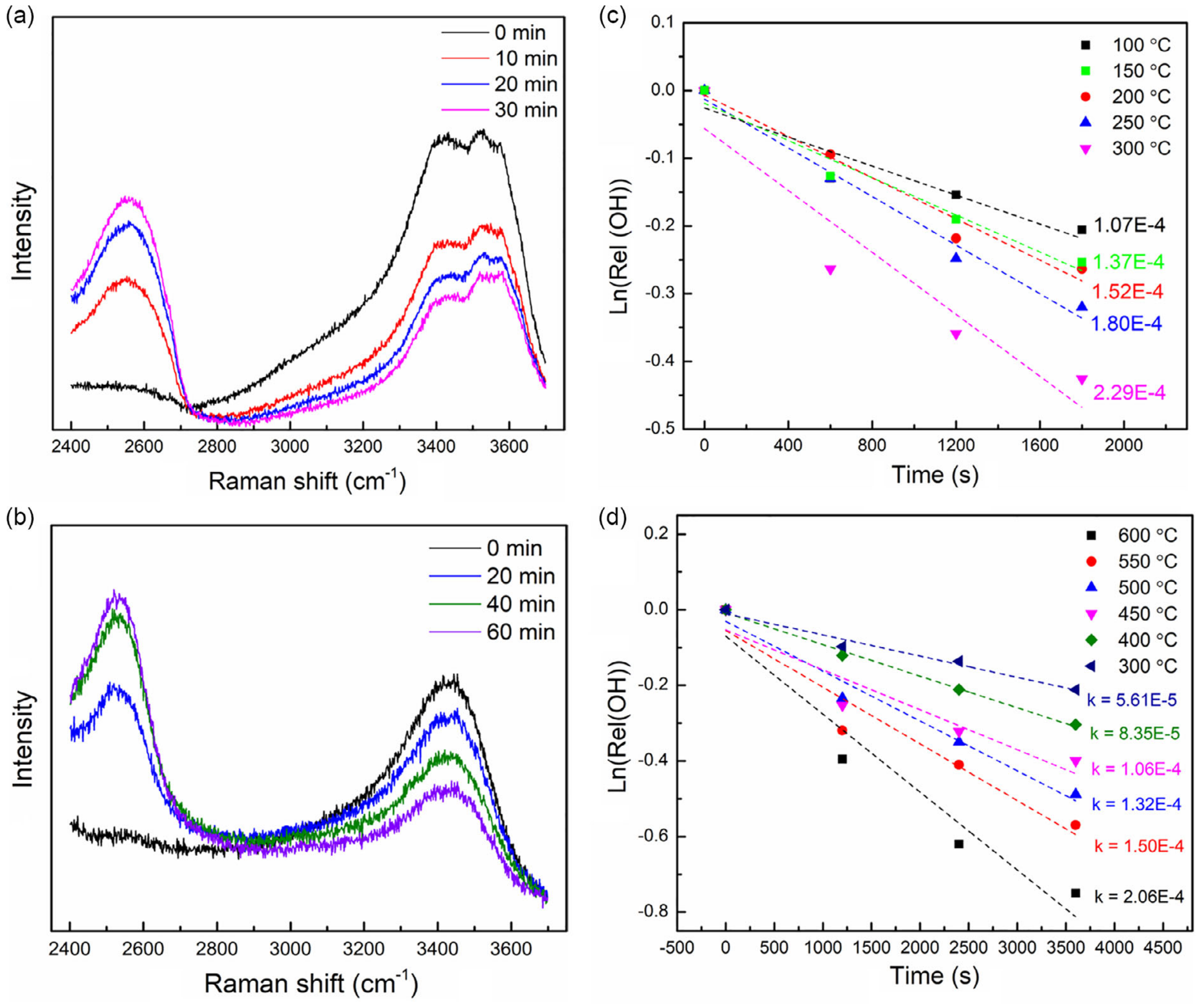

Figure 2. Temporal evolution of Raman spectra of a) nanostructured BCZYYb membrane and b) conventional BCZYYb membrane after switching the atmosphere from Ar–3% H_2O to Ar–3% D_2O at 300 °C; natural logarithm of the integrated relative Raman ν_{OH} intensity in c) nanocrystalline BCZYYb membrane and d) conventional BCZYYb membrane as a function of time of exposure to an atmosphere of Ar–3% D_2O.

Table 1 displays a summary of H/D isotope exchange coefficients (k) in the respective nanocrystalline and conventional BCZYYb membranes. In the designed membrane system, the surface exchange coefficients in a low temperature range (100–300 °C) are comparable or even higher than that in the conventional BCZYYb membrane at a higher temperature range (400–600 °C).

This result indicates that greater grain boundary interfacial area in nanocrystalline samples results in quicker surface exchange rates and concomitant faster proton mobility at the interface in nanoscale perovskite materials compared with "bulk transport" in conventional large-grain-sized membranes.

In addition, the activation energy is much lower in the nanocrystalline BCZYYb membrane, suggesting a lower energy barrier for isotope exchange or proton transport in hydrated layers than in the bulk material, as shown in Figure S4, Supporting Information. More specifically, the surface exchange coefficient in nanocrystalline BCZYYb is nearly four times higher than that in the conventional membrane at 300 °C, which is mainly attributed to the "interfacial effect" or increased grain boundary area in nanocrystalline samples.

The proton concentration in the bulk phase is derived from typical dopant concentrations in high-temperature protonic ceramic conductors. For example, 15 mol% yttrium-doped $BaZrO_3$ has a proton concentration of 10^{21} protons cm^{-3},[42] which is consistent with the proton concentration of nearly 0.7 wt% in dense BCZYYb measured in thermogravimetric (TG) analysis. At low temperatures, the mass loss originated from the desorption of physical absorbed water and surface protonic species.[26,43] In dense BCZYYb membrane, there is negligible absorbed water in the interface due to the small surface area here, 1.4 $m^2\,g^{-1}$, acquired by BET measurements. A much higher proton concentration was achieved in the nanoscale BCZYYb membrane at low temperatures, which was determined by the surface area (3.9 $m^2\,g^{-1}$) and dopant concentration, as shown in **Figure 3**.

As we know, the conductivity (σ, S cm^{-1}), was related to the charge carrier concentration and mobility, as shown in Equation (3).

$$\sigma = nq\mu \tag{3}$$

In the conductivity equation, in which n is carrier density (number of carriers cm^{-3}), q is the electric charge (C), and μ is the mobility ($cm^2\,V^{-1}\,s^{-1}$), An improved proton mobility and increased proton concentration were achieved in the nanoscale BCZYYb membrane compared with the conventional sample, quantitatively suggesting a higher proton conductivity in nanocrystalline BCZYYb compared to the proton transport in conventional BCZYYb through bulk transport at low temperatures, which was exhibited by the lower Ohmic resistance in the single cell's EIS at 300 °C, as shown in **Figure 4**d. The nanocrystalline BCZYYb had a conductivity of 6.0×10^{-4} S cm^{-1}, whereas the conventional BCZYYb had a conductivity of 2.9×10^{-4} S cm^{-1} under working condition at 300 °C.

Table 1. Comparison of H/D isotope exchange coefficients k in nanocrystalline and conventional BCZYYb membrane at different temperatures by in situ Raman spectroscopy.

Nanocrystalline		Conventional	
T [°C]	k [10^{-4} s^{-1}]	T [°C]	k [10^{-4} s^{-1}]
100	1.07	400	0.84
150	1.37	450	1.06
200	1.52	500	1.32
250	1.80	550	1.50
300	2.29	600	2.06

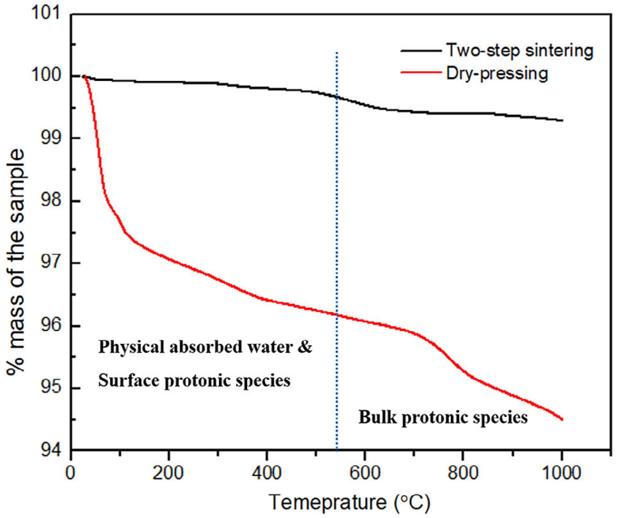

Figure 3. TG curves recorded for the dense BCZYYb membrane prepared by two-step sintering and the nanoscale BCZYYb membrane prepared by a dry-pressing method. Samples were preliminarily protonated under a humidified atmosphere.

In the nanoscale BCZYYb membrane, there is a combined "interface effect" and "bulk effect" for proton transport as demonstrated. From the TG curve of the dry-pressing sample (nanocrystalline BCZYYb), the proton content in the interface is nearly three times larger than that in the bulk. If it is assumed that the proton mobility in the bulk materials of nanoscale BCZYYb is consistent with the dense BCZYYb membrane, the proton mobility in the interface is three times higher than bulk in the nanoscale BCZYYb membrane. Therefore, the interface proton conductivity is nearly an order higher than the bulk proton conductivity in the nanoscale BCZYYb membrane, which is consistent with the observations in our previous study.[26]

Finally, single cells with nanocrystalline BCZYYb as the electrolyte were developed. Figure 4a displays a scanning electron microscopy (SEM) micrograph of a single cell. The electrolyte was nearly 600 μm, and good interfacial contact was achieved between the electrolyte and electrodes. In addition, the electrolyte is gas tight even though it was not calcined at high temperatures.

Figure 4c shows the typical power density (P) as a function of the current density (J) in single cells at 300 °C with BCZYYb and YSZ electrolytes. The single cell with a conventional BCZYYb electrolyte shows similar performance to reported electrolyte-supported single cells at 300 °C.[44] According to the literature, the performance of YSZ-supported single cells could be improved by optimizing the electrode materials. Single cells' performance increased when the electrode changed from dense silver to porous silver, as shown in the insert figure.[44] Moreover, the open circuit

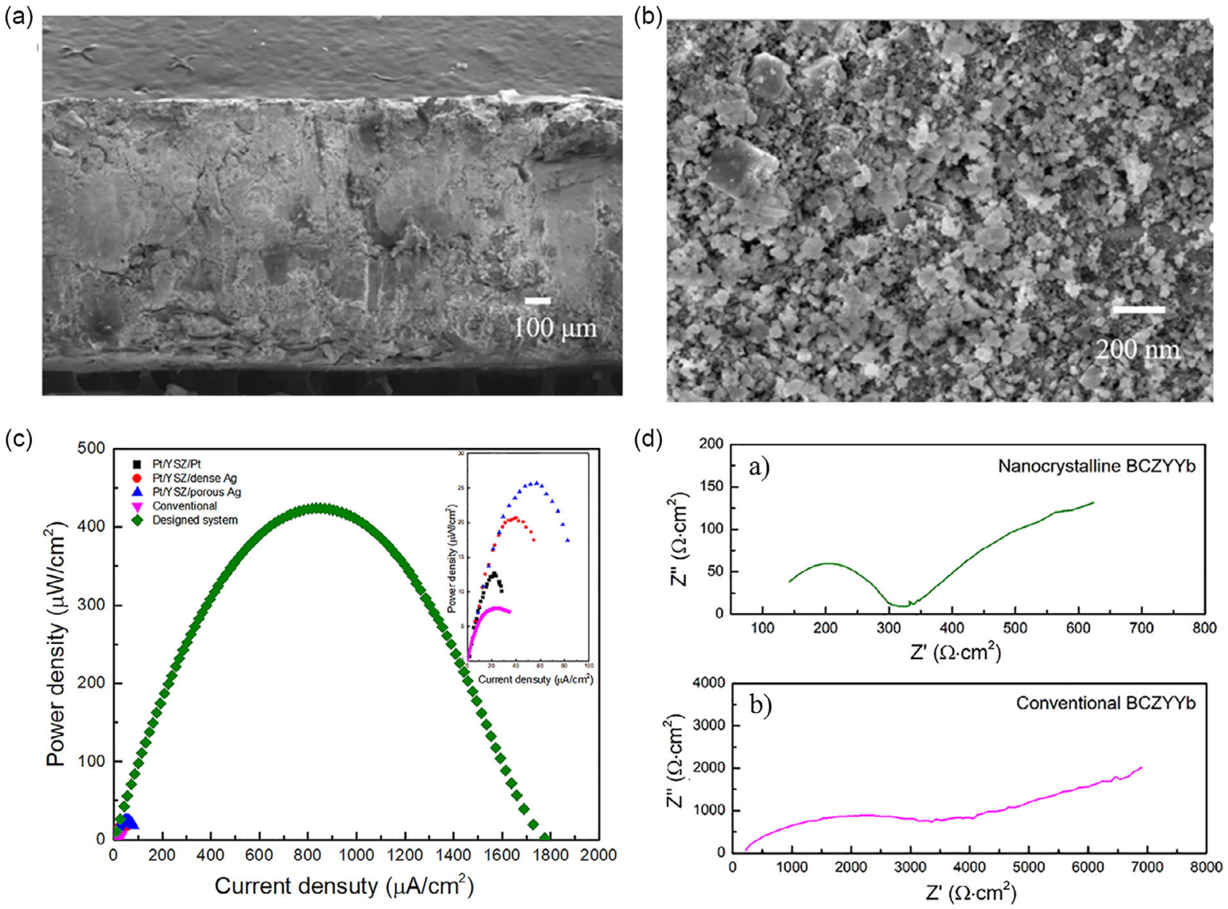

Figure 4. a) Morphology of single cell with nanocrystalline BCZYYb electrolyte by a dry-pressing method, b) nanocrystalline BCZYYb electrolyte in a single cell, c) power density versus current density for single cells with nanocrystalline BCZYYb electrolyte and YSZ-based single cells[44] at 300 °C, and d) Nyquist plots of impedance measured at open circuits with (a) nanocrystalline BCZYYb electrolyte and (b) conventional BCZYYb electrolyte at 300 °C.

voltage is close to the theoretical value (1.1 V), corresponding to the gas-tight membrane identified by SEM and the lack of electronic leakage during the working conditions, as shown in Figure S5, Supporting Information. A much higher single-cell performance was achieved in the designed nanocrystalline membrane system, confirming the potential of applying nanocrystalline BCZYYb as the electrolyte material in low-temperature PCFCs.

Notably, the electrolyte thickness used here is more than 600 µm, which is thicker than the commonly used electrolyte in PCFCs (10–20 µm) and the single-cell performance was limited by the electrode polarization resistance at 300 °C, as shown in Figure 4d. Therefore, the single-cell performance can be further improved by reducing the thickness of the electrolyte and using optimized electrode materials to have comparable performance with the best reported protonic ceramic fuel cells at 300 °C (15 mW cm^{-2} using 110 nm yttrium-doped barium zirconate as the electrolyte).[45]

3. Conclusion

In summary, a new type of proton ceramic conductor was developed by creating more interface areas, in which protons transport not only through the material's bulk, but also in the absorbed water at the interface. In situ Raman spectroscopy and electrical conductivity relaxation were used to directly identify the surface exchange coefficients during hydrogen isotope exchange. The observed surface exchange coefficients in the designed membrane were much higher than the traditional oxidic proton conductors. In addition, single-cell performance was demonstrated using the designed membrane as an electrolyte at low temperatures, indicating potential applications for nanocrystalline membranes as electrolyte materials in low-temperature PCFCs. Based on these results, new material systems were developed that combine interfacial and bulk effects at low temperatures, resulting in a promising new solution for the development of advanced ionic conductors or electrolyte materials through interfacial engineering at the nanoscale.

4. Experimental Section

BCZYYb powder was prepared by a wet chemistry method.[46] Stoichiometric amounts of precursor nitrates were dissolved in distilled water; then critic acid and ethylenediaminetetraacetic acid (EDTA) were added to the solution with metal/citric acid/EDTA ratio of 1:1.5:1.5, working as the chelating agent to assist the combustion process. The precursor solution was heated up in a hot plate to form a gel and then calcined at 900 to 1100 °C for 5 h to remove organic residue from the ash to obtain a pure-phase BCZYYb.

Nanocrystalline BCZYYb membranes were fabricated by a dry-pressing method. The as-prepared BCZYYb powders were pressed in a stainless die at 160 MPa to form the membrane. Conventional dense BCZYYb membranes with large grain size were prepared by a two-step sintering method, as reported in previous work.[47]

A commercial Pt slurry was pasted on one side of Ni foam and desiccated at 100 °C for 20 min and calcined under 5% H_2 to form the Ni foam–Pt composite anode. Commercial $LiNi_{0.8}Co_{0.15}Al_{0.05}O_2$ (LNCA) powder mixed with a dispersant (20 wt% solsperse 28 000 dissolved in terpinol) and binder (5 wt% V-006 (Heraeus) dissolved in terpinol) with a ratio of 15:3:1 to form the LNCA slurry. The LNCA slurry was printed on Ni foam to form the Ni foam–LNCA composite cathode. Then the Ni foam–Pt anode was placed in a stainless die and BCZYYb powder was evenly placed on the electrode and then the Ni foam–LNCA cathode was placed on top of the BCZYYb powder. Finally, an electrolyte-supported single cell was fabricated by a dry-pressing method under 160 MPa. For the conventional sample, the as-prepared LNCA and commercial Pt slurry were printed on the surface of the dense BCZYYb membrane to have electrolyte-supported single cells.

The crystalline structure of the samples was determined using X-ray diffraction (Rigaku TTR-III diffractometer) with a Cu Kα radiation source. The morphologies of BCZYYb membranes were evaluated by SEM (Hitachi S-4800). A TGA Q5000 was used to determine the proton concentration in the BCZYYb membrane. Initially, the protonation process was performed from 600 to 25 °C with 3 wt% H_2O in the furnace. The BET surface analyses were made using nitrogen physisorption (Quantachrome Autosorb iQ Gas Sorption Analyzer).

ECR was conducted to determine the surface exchange coefficients. BCZYYb powder was pressed into rectangular bars at a pressure of 160 Mpa, with the bars having dimensions of $\approx 3.11 \times 4.02 \times 0.81$ mm^3. The conductivity was measured using a digital multimeter (Keithley, 2001 multimeter). A Driertite laboratory gas drier was used to remove the water vapor from the commercial argon. Changes in the gas composition were realized in less than 1 s at a gas flow rate of 100 mL min^{-1} with the change of gas from Ar–3% H_2O to Ar–3% D_2O. The electrical conductivity changed continuously with the relaxation time to reach a new equilibration when the atmosphere was abruptly changed.

Raman scattering spectra were recorded with a Horiba LabRAM HR Evolution Raman confocal microscope equipped with an 800 mm focal length spectrograph and a deep-depleted CCD detector using a 100 mW 532 nm laser with no attenuation, a 50 magnification objective, and 600 groves mm^{-1} diffraction gratings. Spectra corresponded to the accumulation of ten 15 s long scans. Each spectrum was corrected by the prerecorded instrument-specific response to a calibrated white light source, namely, the intensity correction system (ICS). Isotope exchange reactions were performed in a water-cooled hot stage (Linkam, TS1500) by changing the atmosphere from Ar–3% H_2O to Ar–3% D_2O at different temperatures.

Electrolyte-supported single cells were sealed in an alumina tube by a ceramic bond, and silver wires were used as the voltage and current leads on both sides. The electrochemical performance of the single cells was evaluated using hydrogen as the fuel and ambient air as the oxidant. Electrochemical impedance spectra were obtained using an electrochemical workstation (Solartron SI 1287 + 1260) at an alternating current (AC) amplitude of 10 mV in the frequency range from 1 MHz to 10 mHz.

Supporting Information

Supporting Information is available from the Wiley Online Library or from the author.

Acknowledgements

The authors gratefully acknowledge the award DE-NE0008703 from the Department of Energy, Nuclear Energy Research Programs (DOE-NEUP) for project CFA-17-12798: Nanostructured Ceramic Membranes for Enhanced Tritium Management.

Conflict of Interest

The authors declare no conflict of interest.

Data Availability Statement

Research data are not shared.

Keywords

hydrogen isotope exchange, in situ Raman, nanocrystalline membranes, proton transport, protonic ceramic fuel cells

Received: April 22, 2021
Revised: May 24, 2021

---

[1] N. Q. Minh, *J. Am. Ceram. Soc.* **1993**, *76*, 563.
[2] Z. Zhan, *Science* **2005**, *308*, 844.
[3] S. Chu, A. Majumdar, *Nature* **2012**, *488*, 294.
[4] J. Gao, X. Meng, T. Luo, H. Wu, Z. Zhan, *Int. J. Hydrogen Energy* **2017**, *42*, 18499.
[5] C. Duan, R. J. Kee, H. Zhu, C. Karakaya, Y. Chen, S. Ricote, A. Jarry, E. J. Crumlin, D. Hook, R. Braun, N. P. Sullivan, R. O'Hayre, *Nature* **2018**, *557*, 217.
[6] C. Duan, J. Tong, M. Shang, S. Nikodemski, M. Sanders, S. Ricote, A. Almansoori, R. OHayre, *Science* **2015**, *349*, 1321.
[7] J. Gao, Y. Meng, T. Hong, S. Kim, S. Lee, K. He, K. S. Brinkman, *J. Power Sources* **2019**, *418*, 162.
[8] L. Yang, S. Wang, K. Blinn, M. Liu, Z. Liu, Z. Cheng, M. Liu, *Science* **2009**, *326*, 5.
[9] J. Tong, D. Clark, M. Hoban, R. O'Hayre, *Solid State Ionics* **2010**, *181*, 496.
[10] K. D. Kreuer, *Ann. Rev. Mater. Res.* **2003**, *33*, 333.
[11] Y. Zhou, E. Liu, Y. Chen, Y. Liu, L. Zhang, W. Zhang, Z. Luo, N. Kane, B. Zhao, L. Soule, Y. Niu, Y. Ding, H. Ding, D. Ding, M. Liu, *ACS Energy Lett.* **2021**, *6*, 1511.
[12] C. Duan, R. Kee, H. Zhu, N. Sullivan, L. Zhu, L. Bian, D. Jennings, R. O'Hayre, *Nat. Energy* **2019**, *4*, 230.
[13] S. Choi, C. J. Kucharczyk, Y. Liang, X. Zhang, I. Takeuchi, H.-I. Ji, S. M. Haile, *Nat. Energy* **2018**, *3*, 202.
[14] N. Danilov, E. Pikalova, J. Lyagaeva, B. Antonov, D. Medvedev, A. Demin, P. Tsiakaras, *J. Power Sources* **2017**, *366*, 161.
[15] J. Lyagaeva, N. Danilov, G. Vdovin, J. Bu, D. Medvedev, A. Demin, P. Tsiakaras, *J. Mater. Chem. A* **2016**, *4*, 15390.
[16] N. A. Danilov, J. G. Lyagaeva, D. A. Medvedev, A. K. Demin, P. Tsiakaras, *Electrochim. Acta* **2018**, *284*, 551.
[17] M. Shirpour, R. Merkle, J. Maier, *Solid State Ionics* **2012**, *225*, 304.
[18] Y. Yamazaki, R. Hernandez-Sanchez, S. M. Haile, *Chem. Mater.* **2009**, *21*, 2755.
[19] D. Clark, J. Tong, A. Morrissey, A. Almansoori, I. Reimanis, R. O'Hayre, *Phys. Chem. Chem. Phys.* **2014**, *16*, 5076.
[20] J. H. Shim, T. M. Gür, F. B. Prinz, *Appl. Phys. Lett.* **2008**, *92*, 253115.
[21] D. Pergolesi, E. Fabbri, A. D'Epifanio, E. Di Bartolomeo, A. Tebano, S. Sanna, S. Licoccia, G. Balestrino, E. Traversa, *Nat. Mater.* **2010**, *9*, 846.

[22] G. Chen, W. Sun, Y. Luo, Y. He, X. Zhang, B. Zhu, W. Li, X. Liu, Y. Ding, Y. Li, S. Geng, K. Yu, *ACS Appl. Mater. Interfaces* **2019**, *11*, 10642.
[23] G. Chen, Y. Luo, W. Sun, H. Liu, Y. Ding, Y. Li, S. Geng, K. Yu, G. Liu, *Int. J. Hydrogen Energy* **2018**, *43*, 12765.
[24] S. Miyoshi, Y. Akao, N. Kuwata, J. Kawamura, Y. Oyama, T. Yagi, S. Yamaguchi, *Chem. Mater.* **2014**, *26*, 5194.
[25] B. Scherrer, M. V. F. Schlupp, D. Stender, J. Martynczuk, J. G. Grolig, H. Ma, P. Kocher, T. Lippert, M. Prestat, L. J. Gauckler, *Adv. Funct. Mater.* **2013**, *23*, 1957.
[26] J. Gao, Y. Meng, A. Benton, J. He, L. G. Jacobsohn, J. Tong, K. S. Brinkman, *ACS Appl. Mater. Interfaces* **2020**, *12*, 38012.
[27] S. Kim, U. Anselmi-Tamburini, H. J. Park, M. Martin, Z. A. Munir, *Adv. Mater.* **2008**, *20*, 556.
[28] E.-M. Köck, M. Kogler, B. Klötzer, M. F. Noisternig, S. Penner, *ACS Appl. Mater. Interfaces* **2016**, *8*, 16428.
[29] S. Ø. Stub, E. Vøllestad, T. Norby, *J. Phys. Chem. C* **2017**, *121*, 12817.
[30] F. Maglia, I. G. Tredici, G. Spinolo, U. Anselmi-Tamburini, *J. Mater. Res.* **2012**, *27*, 1975.
[31] W. C. Chueh, C.-K. Yang, C. M. Garland, W. Lai, S. M. Haile, *Phys. Chem. Chem. Phys.* **2011**, *13*, 6442.
[32] G. Gregori, M. Shirpour, J. Maier, *Adv. Funct. Mater.* **2013**, *23*, 5861.
[33] Y. Meng, J. Gao, Z. Zhao, J. Amoroso, J. Tong, K. S. Brinkman, *J. Mater. Sci.* **2019**, *54*, 9291.
[34] M. V. Ananyev, A. S. Farlenkov, E. Kh. Kurumchin, *Int. J. Hydrogen Energy* **2018**, *43*, 13373.
[35] A. S. Farlenkov, M. I. Vlasov, N. M. Porotnikova, I. A. Bobrikov, A. V. Khodimchuk, M. V. Ananyev, *Int. J. Hydrogen Energy* **2020**, *45*, 23455.
[36] H. H. Shin, S. McIntosh, *J. Mater. Chem. A* **2013**, *1*, 7639.
[37] A. M. Amado, P. J. A. Ribeiro-Claro, *Faraday Trans.* **1997**, *93*, 2387.
[38] A. M. da Silva, T. Steiner, W. Saenger, J. Empis, J. J. C. Teixeira-Dias, *Chem. Commun.* **1997**, *5*, 465.
[39] T. Norby, Y. Larring, *Curr. Opin. Solid State Materi. Sci.* **1997**, *2*, 593.
[40] C.-S. Tu, R. R. Chien, V. H. Schmidt, S. C. Lee, C.-C. Huang, *J. Phys.: Condens. Matter* **2012**, *24*, 155403.
[41] M. Liu, W. Sun, X. Li, S. Feng, D. Ding, D. Chen, M. Liu, H. C. Park, *Int. J. Hydrogen Energy* **2013**, *38*, 14743.
[42] M. Shirpour, G. Gregori, R. Merkle, J. Maier, *Phys. Chem. Chem. Phys.* **2011**, *13*, 937.
[43] P. Colomban, O. Zaafrani, A. Slodczyk, *Membranes* **2012**, *2*, 493.
[44] C.-C. Yu, J. D. Baek, C.-H. Su, L. Fan, J. Wei, Y.-C. Liao, P.-C. Su, *ACS Appl. Mater. Interfaces* **2016**, *8*, 10343.
[45] J. H. Shim, J. S. Park, J. An, T. M. Gür, S. Kang, F. B. Prinz, *Chem. Mater.* **2009**, *21*, 3290.
[46] M. Shang, J. Tong, R. O'Hayre, *Mater. Lett.* **2013**, *92*, 382.
[47] S. Wang, L. Zhang, L. Zhang, K. Brinkman, F. Chen, *Electrochim. Acta* **2013**, *87*, 194.